RESEARCH ARTICLE

WILEY **NMR** IN BIOMEDICINE

Age-dependent changes in metabolite profile and lipid saturation in dystrophic mice

Brittany Lee-McMullen[1,2] (ID) | Stephen M. Chrzanowski[1] | Ravneet Vohra[1] (ID) |
Sean C. Forbes[3] (ID) | Krista Vandenborne[3] | Arthur S. Edison[2] (ID) | Glenn A. Walter[1,2] (ID)

[1] Department of Physiology and Functional Genomics, University of Florida, Gainesville, FL, USA

[2] Department of Biochemistry and Molecular Biology, Southeast Center for Integrated Metabolomics, University of Florida, Gainesville, FL, USA

[3] Department of Physical Therapy, University of Florida, Gainesville, FL, USA

Correspondence
Glenn A. Walter, Department of Physiology and Functional Genomics, University of Florida, Gainesville, FL 32610-0245, USA.
Email: glennw@ufl.edu

Present Address
Arthur S. Edison, Complex Carbohydrate Research Center, University of Georgia, Athens, GA, USA

Duchenne Muscular Dystrophy (DMD) is a fatal X-linked genetic disorder. In DMD, the absence of the dystrophin protein causes decreased sarcolemmal integrity resulting in progressive replacement of muscle with fibrofatty tissue. The effects of lacking dystrophin on muscle and systemic metabolism are still unclear. Therefore, to determine the impact of the absence of dystrophin on metabolism, we investigated the metabolic and lipid profile at two different, well-defined stages of muscle damage and stabilization in *mdx* mice. We measured NMR-detectable metabolite and lipid profiles in the serum and muscles of *mdx* mice at 6 and 24 weeks of age. Metabolites were determined in muscle in vivo using ^{1}H MRI/MRS, in isolated muscles using ^{1}H-HR-MAS NMR, and in serum using high resolution ^{1}H/^{13}C NMR. Dystrophic mice were found to have a unique lipid saturation profile compared with control mice, revealing an age-related metabolic change. In the 6-week-old *mdx* mice, serum lipids were increased and the degree of lipid saturation changed between 6 and 24 weeks. The serum taurine-creatine ratio increased over the life span of *mdx*, but not in control mice. Furthermore, the saturation index of lipids increased in the serum but decreased in the tissue over time. Finally, we demonstrated associations between MRI-T_2, a strong indicator of inflammation/edema, with tissue and serum lipid profiles. These results indicate the complex temporal changes of metabolites in the tissue and serum during repetitive bouts of muscle damage and regeneration that occur in dystrophic muscle.

KEYWORDS

Duchenne muscular dystrophy (DMD), lipids, metabolism, metabolomics, muscle, neuromuscular disease

1 | INTRODUCTION

Duchenne muscular dystrophy (DMD) is an X-linked recessive disorder with a prevalence of 1 in 5000 live male births.[1] DMD is caused by mutations in the dystrophin gene, which leads to progressive muscle deterioration, loss of functional abilities, and eventually death occurs typically in the third decade of life.[2] Currently there is no cure for DMD, but there have been many promising clinical trials in the past five years.[3-5]

It is clear that the loss of dystrophin has both structural and metabolic consequences. Dystrophin acts to transmit lateral forces and helps to stabilize the muscle membrane during muscle contraction.[6-8] Without dystrophin to stabilize the sarcolemma, eccentric contractions lead to membrane damage initiating chronic bouts of muscle repair and damage.[6] This cycle continues until the healthy muscle is replaced by noncontractile tissue such as lipids and collagen/fibronectin and the cell environment is no longer conducive for muscle regeneration.[9] Additionally, dystrophin also acts to anchor neuronal nitric oxide synthase (nNOS) to the subsarcolemmal space, where localization is important for vasodilation[1] and metabolism.[2]

Many studies have investigated the changes of metabolism secondary to the loss of dystrophin.[10-23] When dystrophin is not functional, there are significant alterations in nitric oxide synthesis,[10] energy metabolism,[11-16] and lipid synthesis.[17-21] Interestingly, investigations of serum[17,18] and muscle biopsies[19-21] have shown alterations in lipid metabolism in both DMD patients and in dystrophic mice, but, to date, there is no clear understanding of the mechanism by which lipids infiltrate the muscle and what corresponding metabolic changes occur systemically. It has been suggested that the muscle lipid infiltration is a consequence of an accumulation of lipids necessary for required membrane repair.[24] Milad et al found that a high-fat diet in mdx-ApoE dramatically worsened fat infiltration and replacement of muscle. One hypothesis was that the circulating molecules are more readily able to diffuse into the muscle cells through the semi-permeable membrane of dystrophin-deficient muscle.[25] Furthermore, they suggest that circulating lipids are potentially significant contributors to the mechanism and progression of DMD pathology. They reason that murine models might exhibit mild phenotypes due to the low plasma lipid levels generally seen in mice. Others have argued that lipid accumulation occurs through mitochondrial dysfunction, which causes the cell to lose its ability to maintain lipid vacuoles in the membrane, and they diffuse into the intercellular space.[26] Although *mdx* mice accumulate less fat than patients with DMD,[27,28] using tissue NMR, we found that there are still significant changes in lipid composition in the muscles of *mdx* mice.[12] To our knowledge, the relationship between serum and muscle lipids in the *mdx* mouse at different stages of disease has not been investigated. Therefore, it is important to obtain a comprehensive set of measurements to improve our understanding of the metabolite equilibrium that exists between tissue and serum in control and dystrophin-deficient muscle at different stages of disease. In addition, it is of great importance to characterize disease-related changes that can be quantified and used to track disease progression through an affordable, easy to acquire blood test.

The *mdx* mouse model, which lacks functional dystrophin, is the most commonly studied mouse model in DMD; however, the phenotype is less severe than in humans lacking dystrophin, in part to the upregulation of utrophin in mice[29] and the tremendous regenerative capacity of mice. Despite this, *mdx* mice demonstrate well-characterized stages, including an initial stage characterized by muscle damage and inflammation at four to six weeks. This is followed by a "recovery" phase in which regeneration appears to match degeneration from approximately 24 to 65 weeks. During the later stages of life, lipid infiltration, fibrosis, and necrosis become more predominant.[30]

The objective of this study was to investigate changes in muscle and serum metabolites and lipids from *mdx* mice at both the initial muscle damage phase (6 weeks) and during the recovery phase (24 weeks of age). We discovered abnormalities in lipid and glucose metabolism of the *mdx* mouse which may prove useful for mechanistic insights for translational investigations in DMD.

2 | EXPERIMENTAL

2.1 | Animals

C57BL/10ScSn-DMD *mdx* mice (*mdx*) and age-matched C57BL/10ScSn (controls) were purchased from Jackson Laboratories (Bar Harbor, ME, USA). The University of Florida's institutional animal care and use committee (IACUC) approved the experimental protocol for this study. All animals were maintained with a 12-hour light–dark cycle, at 22.2°C and 42% humidity at the University of Florida Animal Facilities, which are approved by the Accreditation of Laboratory Animal Care.

2.2 | Study design

Both *mdx* and control (C57BL10) mice were obtained at 4 weeks of age and raised to either 6 [*mdx* (*n* = 6), control (*n* = 5)] or 24 weeks old [*mdx* (*n* = 10), control (*n* = 8)]. At each time point (6 or 24 weeks), in vivo mouse lower leg hindlimb data were collected using T_2-magnetic resonance imaging (MRI), followed by blood and tissue collection when the animals were sacrificed. At sacrifice, while administering 2% isoflurane for anesthesia, 200 μL of blood were collected by submandibular puncture from randomized animals to reduce any potential order effect and bias. Blood was allowed to sit at room temperature for 30 minutes to clot, then was centrifuged to extract serum. The gastrocnemius muscles were extracted,

flash-frozen and stored at −80°C until further analysis. The mice were then euthanized as per approved IACUC protocols. All experiments were performed in the morning (from 8–10 AM; food was removed from cages one hour before euthanizing).

2.3 | In vivo imaging and spectroscopy

Magnetic resonance imaging and spectroscopy (MRS) were performed on an 11.1-T horizontal bore magnet (Magnex) equipped with an Agilent spectrometer. Mice were anesthetized with 3% isoflurane mixed with oxygen followed by maintenance at 0.5–1% isoflurane throughout the scanning. Temperature (maintained with a circulated warm water heating pad) and respiration were monitored throughout the entire scanning period using a fiber optic small animal physiological monitoring device (SAI; Stoney Brook). The lower hindlimbs of the *mdx* (6-week, *n* = 6; 24-week, *n* = 10) and control (6-week, *n* = 5; 24-week, *n* = 8) mice were inserted into a 2.0-cm internal-diameter, custom-built ^1H solenoid coil, up to the knee. For T_2-weighted MR images, multiple slice, single spin-echo images were acquired with a repetition time (TR) of 2000 ms, echo times (TE) of 14 ms and 40 ms, a field of view of 10–20 mm^2, slice thickness of 0.5–1 mm, and with an acquisition matrix of 128 x 256 for two signal averages. The T_2 decay was fit to a single-exponential curve. A 1 x 2 x 2 mm^3 voxel was positioned for spectroscopy in the gastrocnemius located in the posterior compartment of the lower leg, where care was taken to avoid other muscles. These voxels were placed as precisely as possible between mice. Spectroscopy was performed using a localization by adiabatic selective refocusing (LASER)[31] pulse sequence with a TE of 14 ms, TR of two seconds, 1024 spectral data points, a spectral width (SW) of 15 ppm, and using the WET[32] water suppression sequence.

2.4 | Solution NMR of serum

Serum was separated from the red blood cells by allowing samples to sit at room temperature for 30 minutes before centrifugation for 15 minutes at 10 000 g at 4°C. Samples were then transferred to an Eppendorf tube, flash-frozen in liquid nitrogen and stored at −80°C. At the time of analysis, samples were thawed and approximately 100 μL serum was lyophilized and re-suspended in 40 μL 99% D_2O (Cambridge Isotope Laboratories, Tewksbury, MA, USA) and transferred into 1.5 mm NMR tubes (Norell, Morganton, NC). One-dimensional ^1H and ^{13}C spectra were collected at a controlled temperature of 25° C on an Agilent VNMRS-600 spectrometer using a custom 1.5 mm ^{13}C high temperature superconducting (HTS) probe.[33]

One-dimensional ^1H data were acquired in approximately 18 minutes using a Carr-Purcell-Meiboom-Gill (CPMG) sequence, which was utilized to remove the macromolecule and lipoprotein signal contribution due to T_2 decay, resulting in a flat baseline.[34,35] Data were recorded with the following parameters: SW of 9615.4 Hz, a 2.0 s relax delay, a 90-degree initial pulse, a train of 124 x 180-degree CPMG pulses with a 1 ms inter-pulse delay, and a 2.0 s acquisition time and 128 scans.

1D ^{13}C spectra were collected in approximately two hours under conditions that favor nuclei with short T_1 relaxation times in order to maximize overall sensitivity and minimize measurement time, as described previously.[36] Protein contribution was found to affect the baseline in ^{13}C spectra and therefore a ^{13}C CPMG sequence with a 90-degree excitation pulse followed by a train of 18 individual 180-degree pulses with a 1 ms inter-pulse delay was used. The ^{13}C CPMG sequence used a 60° excitation pulse with a very short 0.1 s relaxation delay (D1) at the start of each experiment, a 0.8 s acquisition time, a 212 ppm (32 051.3 Hz) spectral window, and a carrier frequency of 98.0 ppm at a frequency of 150.79 MHz. ^1H was decoupled and allowed to build up an nuclear Overhauser effect (NOE) at 599.68 MHz with a power of 37 dB using a continuous WALTZ-16 sequence.

2.5 | HR-MAS NMR on ex vivo gastrocnemius muscle

The gastrocnemius muscle of the control and *mdx* mice at 6 (*mdx* = 6, control = 5) and 24 weeks (*mdx* = 10, control = 8) was analyzed using high-resolution magic-angle spinning (HR-MAS) NMR. Data were acquired using a 4 mm HR-MAS probe on a Bruker 600 MHz spectrometer (AVIII) running Topspin 3.2 software. Sample preparation and data acquisition followed the protocols from Beckonert et al.[37] In addition, the wet weight of the muscle was measured and used for normalization. The magic angle was optimized and set for all samples using potassium bromide (KBr). Pulse calibration, tune, match and manual shimming were performed for each muscle sample. One-dimensional Nuclear Overhauser effect spectroscopy (NOESY) with water presaturation was acquired with a total of 128 scans, a SW of 12 ppm, 16 000 complex data points, a relaxation delay of two seconds and a NOESY mixing time of 90 ms. All samples were acquired at 4°C and in under 30 minutes as per protocol.

2.6 | Data processing

In vivo imaging and spectroscopy was used to measure the muscle T_2 and muscle metabolites, respectively, in the gastrocnemius. An average of six slices of in vivo MRI images were used to measure T_2 values using echo times of 14 and 40 ms.[38] In vivo spectra were processed and analyzed using Mnova NMR software [MestReNova (Mnova) NMR, version 11.0.3, Mestrelab Research S. L., Santiago de Compostela, Spain; www.mestrelab.com, 2017]. Spectra were apodized, zero-filled twice, Fourier-transformed, phased, baseline-corrected, referenced using the in vivo creatine peak at 3.02 ppm, aligned and normalized to water. Each metabolite was quantified by integration of resolved peaks.

HR-MAS and solution NMR spectra were processed using NMRPipe.[39] Spectra were apodized (cosine squared for ^{1}H and exponential with 2 Hz line broadening for ^{13}C), zero-filled twice, Fourier-transformed, phased, and baseline-corrected. ^{1}H spectra were referenced to the lactate peak at 4.1 ppm. ^{13}C spectra were referenced to the anomeric carbon glucose peak at 98.64 ppm. Further processing and analysis of NMR spectra were performed using an in-house MATLAB metabolomics toolbox.[40] Spectra were referenced, aligned using the peak alignment fast Fourier transform (PAFFT) algorithm[41] and normalized using Probabilistic Quotient Normalization (PQN).[42] PQN is a method used to normalize spectra by finding the most probable dilution factor using the distribution of quotients of amplitudes of each test spectrum compared with a reference spectrum (average spectrum). Metabolites were quantified using integration of resolved ^{1}H resonances with chemical shift ranges defined in Table S1 (tissue) and Table S2 (serum). The polyunsaturation index (*pi*) and unsaturation index (*ui*) were calculated according to Mosconi et al[43] using the following equations:

$$pi = \frac{Lipid\ B}{\left(\frac{2}{3}\right) Lipid\ A} \tag{1}$$

$$ui = \frac{Lipid\ C}{\left(\frac{2}{3}\right) Lipid\ A} \tag{2}$$

where Lipid A (**CH3**)is the peak at 0.9 ppm, Lipid B (HC=CH-**CH2**-HC=CH) is the peak at 2.75 ppm, and Lipid C (**HC=CH**) is the peak at 5.4 ppm.

2.7 | Data analysis

Multivariate analyses were conducted using nonlinear iterative partial least squares (NIPALS) principle component analysis (PCA)[44] and partial least squares discriminant analysis (PLS-DA)[45] using our in-house MATLAB metabolomics toolbox.[40] Targeted comparisons were analyzed using Graphpad Prism version 6. Quantified metabolites were tested for normality using the Shapiro–Wilk test.[46] Comparisons between controls and *mdx* at both ages determined to be normal were analyzed using a one-way ANOVA and a Bonferonni correction. Comparisons between *mdx* and controls at both ages that were not determined as normal using the Shapiro–Wilk normality test were compared using a Mann–Whitney test that was corrected for multiple comparisons. Correlations of metabolite and MR parameters were determined using a linear correlation matrix, in MATLAB (corrcoef), which calculated both the correlation coefficients and *P*-values and used a false discovery rate (FDR) of 0.05 to correct for the multiple comparisons.

3 | RESULTS

3.1 | In vivo MR characterization of muscle

We used MRI T_2–weighted imaging to visualize and to quantify the state of disease in vivo in *mdx* mice at 6 and 24 weeks of age. Figure 1 shows representative MR images of hind limbs from 6-week control (A; $n = 5$) and *mdx* (B; $n = 6$) mice, and 24-week control (C; $n = 8$) and *mdx* (D; $n = 10$) mice. Control mice demonstrated homogenous signal throughout the muscle, indicating healthy muscle tissue. The *mdx* mice showed regions of hyperintense signal, symptomatic of muscle damage and/or inflammation. The MRI T_2 was calculated from the posterior compartment (outlined in yellow) of the hind limb of each mouse to quantify the amount of damage/inflammation (Figure 1E). We found that the posterior hindlimb mus-cle T_2 of 6-week-old *mdx* mice were significantly ($P = 0.0003$) higher (37.4 ± 1.5 ms) than that of 6-week-old controls (27.3 ± 1.8 ms), 24-week-old controls (23.8 ± 0.3 ms) and 24-week-old *mdx* (26 ± 1.3 ms) (Figure 1E). The muscle T_2 from the 24-week-old *mdx* mice was significantly ($P = 0.01$) higher than that of 24-week-old control mice. There was no significant difference between 6- and 24-week controls (Figure 1E). Figure 1F shows a representative localized ^{1}H spectrum from a voxel (represented as a yellow square) in the posterior compartment of the hind limb, from which creatine (Cr), taurine (Tau) and a histidine-containing derivative (HCD) were quantified for all mice. An overlay of all spectra is included as Figure S1. There were no significant changes between groups in Cr, Tau or HCD. Consistent with previous reports in *mdx* mice,[47,48] the in vivo muscle lipid content was low and below the level necessary to reliably calculate an in vivo *pi* and *ui*.

3.2 | Multivariate global analysis of control and dystrophic mice using ^{13}C spectra

^{13}C spectra of control and dystrophic serum at both 6 and 24 weeks were used to perform PCA to identify the largest variation between the cohorts. Figure 2A shows a PCA plot where there is a strong separation of *mdx* from controls at 6 weeks but less so at 24 weeks. PCA of the ^{13}C spectra of the *mdx* mouse serum (Figure 2B) separated 6-week *mdx* from the 24-week *mdx* serum spectra using PCA (verified with PLS-DA

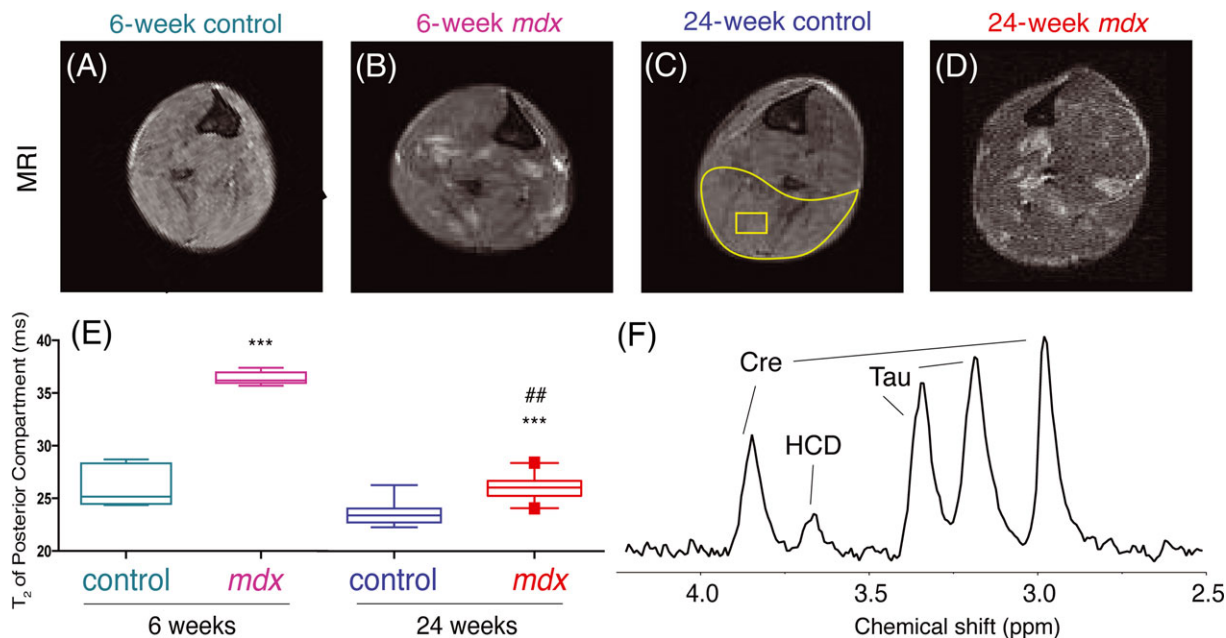**FIGURE 1** Characterization of disease state with MRI T_2. MRI images of the hind limb (A)-(D) of 6-week control (A), 6-week *mdx* (B), 24-week control (C) and 24-week *mdx* (D), respectively. MRI T_2 was taken from an area of interest (yellow area circling muscle) in the posterior compartment of the hind limb (E). A voxel (yellow square) was placed in the posterior compartment of the lower hind limb for quantification of in vivo metabolites using MRS (F). Significance was determined by corrected $P \le 0.05$ or lower. Comparisons to 6-week controls with $P < 0.001$ are denoted with ***. Comparisons to 6-week *mdx* with $P < 0.01$ are denoted with ##. Abbreviations: Cre, creatine; tau, taurine peaks; HCD, histidine-containing derivatives

with a $Q^2 = 0.82$, $R^2 = 0.98$). The loadings plot for principle component (PC) 2 reveals that peaks related to linoleic acid (fatty acids) showed a greater association with 6-week *mdx* and glucose was more associated with the 24-week-old mice (Figure 2C). To guide the eye, the BioMagResBank[49] reference spectra of linoleic acid and glucose are displayed above and below the loadings spectrum, respectively. Peaks for both linoleic acid and glucose were also verified using 2D heteronuclear single quantum correlation (HSQC) spectroscopy (Figure S2).

3.3 | Quantification of serum glucose and lipids

Figure 3 shows the overlay of all ^{1}H NMR serum spectra from dystrophic and control mice at both 6 and 24 weeks of age with inset expansions of lipid and glucose peaks. Integration of A (0.9 ppm), B (2.75 ppm) and C (5.4 ppm) lipid peaks were used to calculate the *pi* (Equation 1) and *ui* (Equation 2) in the lipids.[43] Total lipids (Figure 4A) and *ui* (Figure 4B) were significantly ($P < 0.0001$, $P < 0.01$, respectively) higher in the 6-week-old *mdx* mice compared with age-matched controls, but this was not seen at 24 weeks. The *pi* in the 6-week-old *mdx* mice were lower ($P < 0.01$) than that of the 6-week-old controls, but still higher than both the 24-week-old *mdx* and controls ($P < 0.0001$ for both) (Figure 4C). Glucose levels in the 6-week-old *mdx* mice were significantly ($P < 0.01$) lower than 6-week-old controls (Figure 4D). Conversely, 24-week-old control and *mdx* mice had significantly higher glucose than controls and *mdx* at 6 weeks (Figure 4D).

3.4 | Tissue metabolite comparison at different ages

The metabolic profile of gastrocnemius muscle from both 6- and 24-week-old control and *mdx* mice was determined using ^{1}H HR-MAS NMR. Table S1 summarizes the metabolites, the ppm range used to integrate each metabolite and normalized quantifications (with standard deviations) of both the *mdx* and controls at each age. The taurine-creatine ratio (Figure 5A, $P = 0.009$), and *ui* (Equation 2) (Figure 5B, $P = 0.035$) in the lipids significantly changed between the two ages in *mdx* mice only, but remained unchanged within controls at different ages. This suggests that these metabolic changes are related to the state of the disease in the *mdx* and not merely an effect of age.

3.5 | Correlations of metabolites between serum and tissue

A correlation matrix of pairwise comparisons was made between five tissue metabolites, eight serum metabolite/metabolite ratios, two in vivo metabolites and in vivo T_2 in both controls (left) and *mdx* (right) (Figure 6). The control matrix showed zones of strong and significant correlations
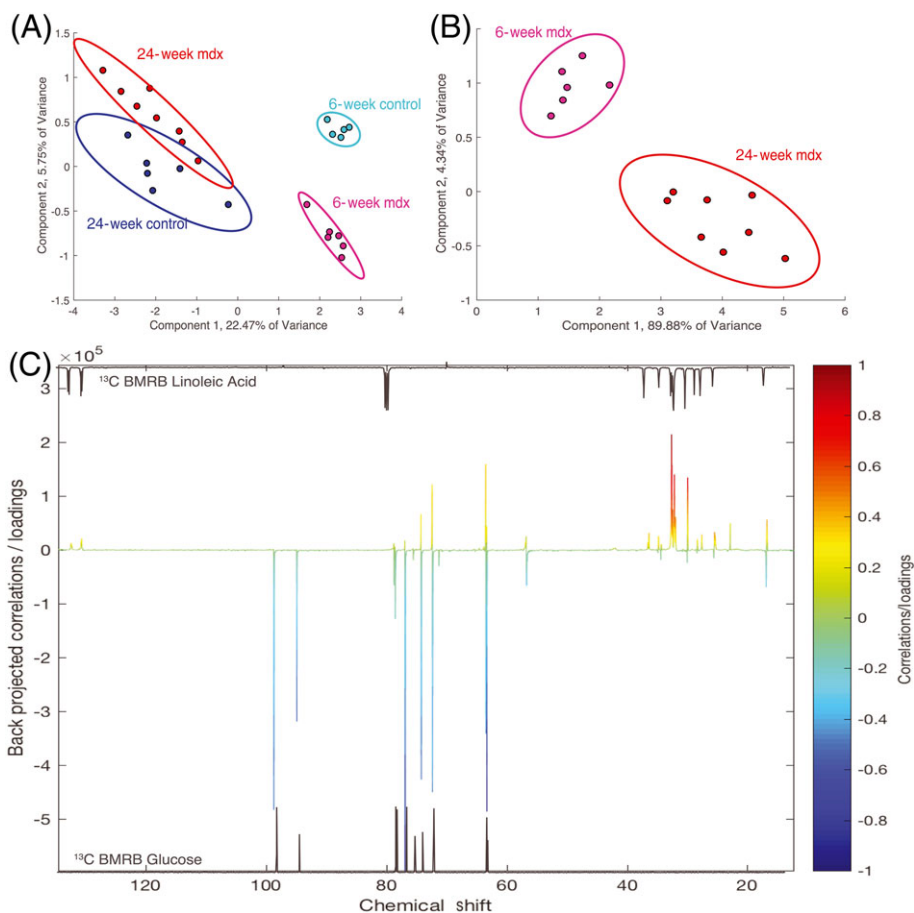
FIGURE 2 PCA of serum ^{13}C NMR spectra can differentiate control and *mdx* at different ages. (A) PCA plot of all groups; (B) PCA of *mdx* at 6 weeks and 24 weeks of age demonstrate the separation on the second component. In (C), the loadings plot of PC 2 showing the 6-week (positive) separate based on lipids and the 24-week (negative) separate based on glucose. Spectra located on the top and bottom BMRB standard spectra (shown on the top and bottom of Figure C) that reveal the similar peaks to the compounds separated out in the loadings plot
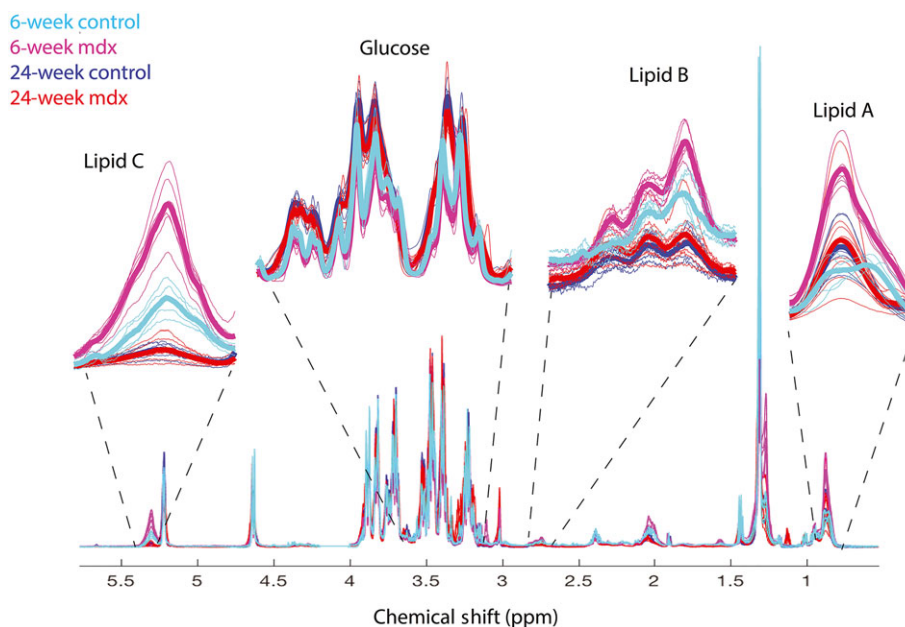

FIGURE 3 Serum ^{1}H spectra indicating peaks of interest. Spectra from control (teal and blue) and *mdx* (pink and red) mice at 6 and 24 weeks. Large changes found in the ^{1}H are magnified to demonstrate the differences. Thin lines are from individual mice, and the bold lines are the mean for each group
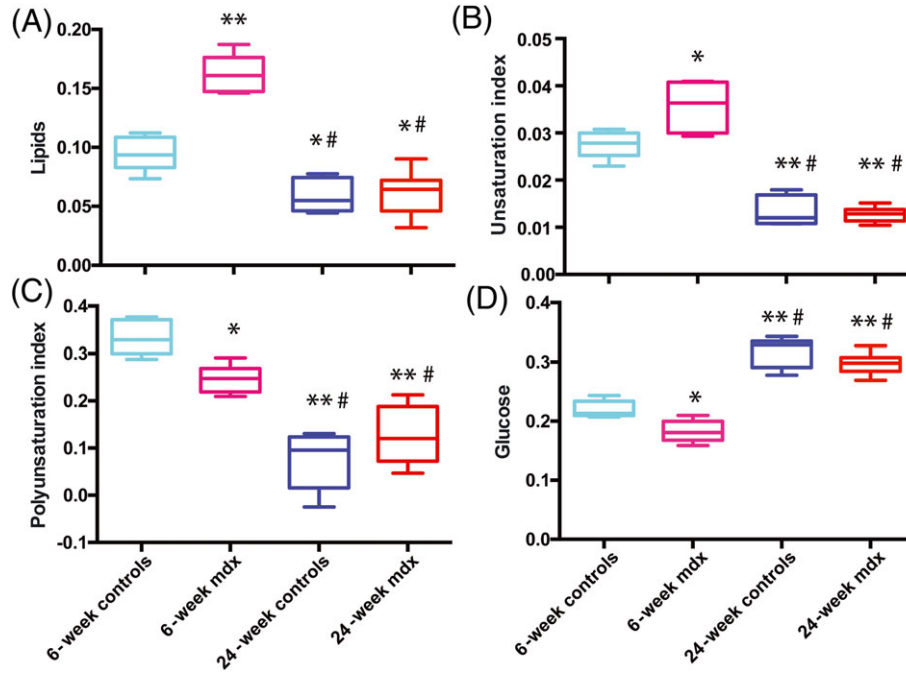
FIGURE 4 Quantification of serum metabolites. Relative abundance quantification from the ^{1}H spectra of lipids and glucose in the serum of control and *mdx* mice at both 6 and 24 weeks of age. Significance was defined as $P < 0.05$. Comparisons with 6-week controls with $P < 0.01$ are denoted with *. Comparisons with 6-week controls with $P < 0.001$ are denoted with **. Comparisons with 6-week *mdx* with $P < 0.001$ are denoted with #. Comparisons with 24-week controls with $P < 0.01$ are denoted with †
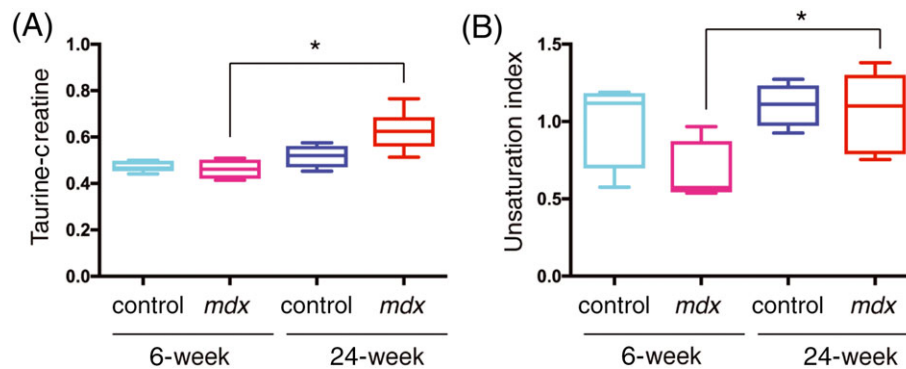

FIGURE 5 Tissue metabolites that change in *mdx* at different ages. Quantification from the ^{1}H HR-MAS spectra of tissue from control and *mdx* mice at both 6 and 24 weeks of age. Significance was determined by $P = 0.05$. Comparisons with 6-week controls with $P < 0.05$ are denoted with *

($r > 0.50$, $P < 0.05$) within the serum metabolite group and within tissue metabolites separately. In the tissue, the lipid peak at 2.1 ppm (HC=CH-CH2) and glycine were the only two metabolites that demonstrate a relationship ($r > 0.6$, $P < 0.05$) with serum metabolites.

Similarly, in *mdx* mice there was also a strong ($r > 0.6$) and significant ($P < 0.001$) positive relationship between glycine and serum metabolites but this was not seen for the lipid peak at 2.1 ppm. Compared with controls, the *mdx* showed no relationship between the peak at 3.0 ppm (most likely an amino acid derivative but this could not be definitively identified by 2D NMR[36]) and alanine with the rest of the serum metabolites. Conversely, there were stronger relationships ($r > 0.6$; $P < 0.01$) between the serum branched chain amino acids (BCAA) and glycine with serum lipids, than was observed in controls. The *mdx* mice showed a strong negative correlation ($r > 0.6$, $P < 0.005$) between the serum peak at 3.0 ppm and the in vivo taurine, whereas no such relationship was seen in controls. However, the most striking contrast was that *mdx* in vivo T_2 strongly correlated ($r > 0.5$; $P < 0.001$) to both tissue and serum lipid measurements, but almost no relationship was observed between control T_2 and lipid measurements. Since MRI T_2 has proven to be a reliable marker for inflammation/damage in *mdx* mice,[38] these data suggest serum and tissue lipid saturation alterations have a relationship to MRI T_2 and, potentially, disease progression or state.
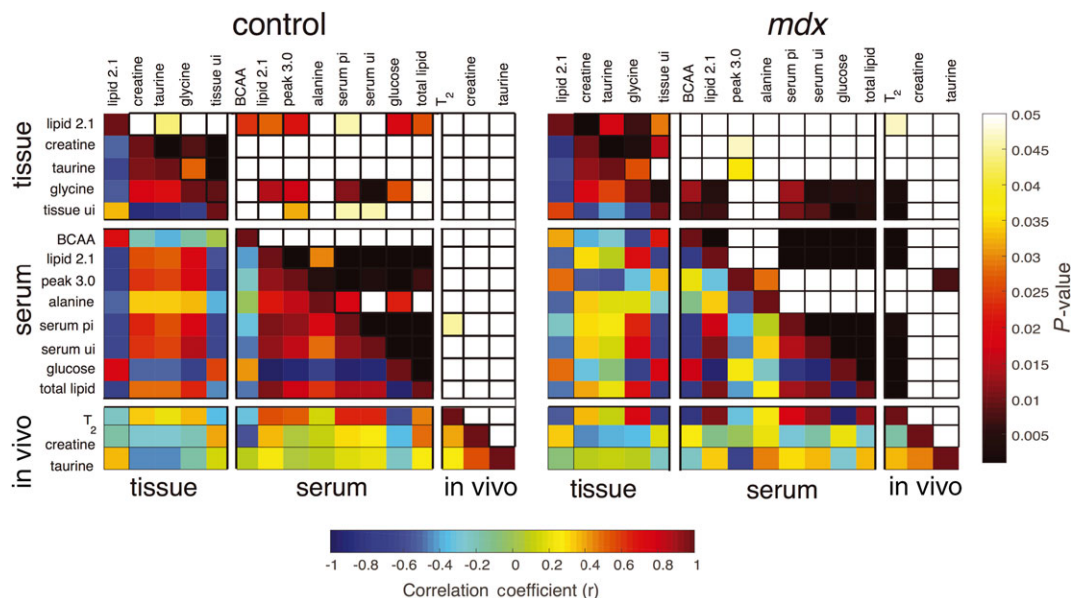
FIGURE 6 Correlations between serum and tissue measurements. The lower left of each correlation matrix are the correlation coefficients for each comparison which are labeled on the left and at the top. The upper-right portion of each correlation matrix are the P-values for the paired comparison. The scale bar at the bottom of the figure corresponds to the correlations and the one on the right represents the corresponding P-values. Each metabolite is grouped into tissue, serum or in vivo, denoted on the left-hand side

4 | DISCUSSION

In this study, tissue and serum NMR were used to investigate the metabolite and lipid profile in *mdx* mice during both the initial muscle damage phase (6 weeks) and during the recovery phase (24 weeks of age). We found strong associations between the lipid profiles in serum with both tissue metabolites and MRI T_2. MRI T_2 can be elevated by increased inflammation and lipid composition, both of which are present in dystrophic mice[38] and individuals with DMD.[50-55] As *mdx* mice age, upregulation of utrophin partially compensates for the loss of dystrophin and ameliorates disease phenotypes,[56,57] shown previously by both histology and MRI.[38] Using MRI T_2, ex vivo tissue HR-MAS and solution NMR of the serum, we are able to show that systemic lipid changes of *mdx* mice correlate with state of disease.

Correlations between serum metabolites, tissue metabolites and in vivo measurements were paramount in determining the systematic alterations occurring in lipids throughout disease. Measured lipids between both the tissue and serum had strong and significant correlation to in vivo MRI T_2. However, it is important to point out that the tissue *ui* is negatively correlated with MRI T_2, whereas serum lipids (*pi*, *ui* and total lipids) all positively correlate with MRI T_2. Altered lipid saturation in the *mdx* mice returned to control levels by 24 weeks, the same time that utrophin is upregulated and disease symptoms are ameliorated. The metabolic profile we observed suggests that the initial bout of damage includes elevated levels of lipids in the serum as damage and repair are occurring within the muscle. As lipids in the serum reduce by 24 weeks, the increase of lipid in the tissue may be coming from the overproduction of lipids to repair cell membrane after damage, as previously suggested.[24] Infiltration of lipids from the circulating blood has previously been suggested by Milad et al[25] as a means to infiltrate leaky muscles. However, the exact mechanism by which fatty tissue infiltrates and replaces muscle tissue is still unclear and needs to be further investigated.

We found that the amount of total lipid increased during the initial wave of muscle damage in 6-week-old mice. However, not all types of lipids increased equally. Others have shown that lipid composition in the muscle and blood of patients with DMD is altered.[12,17-20,58] Following repeated bouts of muscle damage, the contractile tissue of the muscle is replaced by fibrofatty tissue.[23,59,60] We found that the *ui* increased but the *pi* decreased in 6-week-old *mdx* mice compared with controls. These findings are consistent with Gillet et al,[19] who found similar changes in lipid saturation between 3-week-old *mdx* and control mice using 2D NMR. Linoleic acid was higher in controls than in *mdx* mice. In DMD muscle, it has been recently shown by Srivastava et al[23] that linoleic acids are significantly reduced in DMD muscle compared with normal/control individuals. Alterations in polyunsaturated fatty acids in erythrocytes from DMD patients[61] have also been reported. These data demonstrate that in addition to changes in total muscle lipids, there are also systemic lipid changes in people with DMD. Changes in muscle and membrane lipid composition during muscle damage and recovery have been documented both in vivo[19,48] and in vitro.[19] For example, Gillet et al[19] observed that changes in linoleic acid track with membrane fusion and skeletal muscle differentiation and recovery.[19,24] Differences in lipid composition have also been observed in areas of muscle damage in *mdx* muscle using an imaging mass spectrometry technique.[62]

Our observation that tissue taurine levels were associated with lipid composition and MRI T_2 is consistent with other reports of changes in taurine during muscle regeneration[63] and renormalization following steroid treatment.[64] Changes in choline and taurine levels following acute muscle damage in *mdx* mice have been observed in vivo using ^{1}H MRS spectroscopy and validated by histology.[48] In a comparison of injured

and uninjured muscles from *mdx* mice, taurine decreased by 17% and choline increased by 25% in injured muscles. In wildtype mice, intramyocellular lipids and total muscle lipid levels increase significantly with injury.[48] Taurine has consistently been shown to be altered in dystrophic muscles.[11-13,63,64] Overall, the altered taurine-creatine levels in *mdx* vs control muscle suggests that taurine could be a useful biomarker for dystrophic muscle damage.[11-13,63,65]

We also observed a negative correlation between serum glucose and MRI T_2 and serum lipids. Glucose levels were lower during the period of severe muscle damage in *mdx* compared with controls but were not different at 24 weeks of age. Previous studies in the literature[66-68] have shown alterations in blood glucose and insulin resistance in preclinical models of muscular dystrophy and in DMD patients. However, it should be noted that our mice were not fasted for 12 hours prior to sacrifice and therefore this could interfere with interpretation of the data. In addition, we did not examine mice at ages older than 24 weeks and it is possible that blood glucose levels may differ at those ages. Future studies examining *mdx* mice at multiple time points postfasting at different ages could provide further mechanistic insight into glucose metabolism in dystrophic mice.

In conclusion, we found a complex, temporal interplay between metabolism in the tissue and serum during periods of elevated muscle damage/inflammation and recovery in dystrophic muscle. Specifically, metabolic profile changes and systemic lipid saturation in *mdx* mice were altered at different ages vs controls. Correlations between serum lipids to tissue lipids and in vivo MRI T_2 suggest that lipid saturation in serum is a potential means to monitor disease state in dystrophic muscle, and this is obtainable in an uncomplicated, minimally invasive, and translational manner.

ACKNOWLEDGEMENTS

ORCID

Brittany Lee-McMullen 🔵 https://orcid.org/0000-0002-8905-6021
Ravneet Vohra 🔵 https://orcid.org/0000-0001-6258-2710
Sean C. Forbes 🔵 https://orcid.org/0000-0002-5258-8104
Arthur S. Edison 🔵 https://orcid.org/0000-0002-5686-2350
Glenn A. Walter 🔵 https://orcid.org/0000-0002-7346-2244

REFERENCES

1. Mendell JR, Lloyd-Puryear M. Report of MDA muscle disease symposium on newborn screening for Duchenne muscular dystrophy. *Muscle Nerve.* 2013;48:21-26.

2. Bushby K, Finkel R, Birnkrant DJ, et al. Diagnosis and management of Duchenne muscular dystrophy, part 2: implementation of multidisciplinary care. *Lancet Neurol.* 2010;9:177-189.

3. Bushby K, Finkel R, Wong B, et al. Ataluren treatment of patients with nonsense mutation dystrophinopathy. *Muscle Nerve.* 2014;50:477-487.

4. Fairclough RJ, Wood MJ, Davies KE. Therapy for Duchenne muscular dystrophy: renewed optimism from genetic approaches. *Nat Rev Genet.* 2013;14:373-378.

5. Konieczny P, Swiderski K, Chamberlain JS. Gene and cell-mediated therapies for muscular dystrophy. *Muscle Nerve.* 2013;47:649-663.

6. Ervasti JM, Campbell KP. A role for the dystrophin-glycoprotein complex as a transmembrane linker between laminin and actin. *J Cell Biol.* 1993;122:809-823.

7. Ervasti JM, Ervasti JM, Ohlendieck K, et al. Deficiency of a glycoprotein component of the dystrophin complex in dystrophic muscle. *Nature.* 1990;345:315-319.

8. Ervasti JM, Campbell KP. Membrane organization of the dystrophin-glycoprotein complex. *Cell.* 1991;66:1121-1131.

9. Boldrin L, Zammit PS, Morgan JE. Satellite cells from dystrophic muscle retain regenerative capacity. *Stem Cell Res.* 2015;14:20-29.

10. Tidball JG, Wehling-Henricks M. Nitric oxide synthase deficiency and the pathophysiology of muscular dystrophy. *J Physiol.* 2014;592:4627-4638.

11. Griffin JL, Rosiers Des C. Applications of metabolomics and proteomics to the mdx mouse model of Duchenne muscular dystrophy: lessons from downstream of the transcriptome. *Genome Med.* 2009;1:32.

12. Griffin JL, Williams HJ, Sang E, Nicholson JK. Abnormal lipid profile of dystrophic cardiac tissue as demonstrated by one- and two-dimensional magic-angle spinning (1)H NMR spectroscopy. *Magn Reson Med.* 2001;46:249-255.

13. Griffin JL, Sang E, Evens T, Davies K, Clarke K. Metabolic profiles of dystrophin and utrophin expression in mouse models of Duchenne muscular dystrophy. *FEBS Lett.* 2002;530:109-116.

14. Kuznetsov AV, Winkler K, Wiedemann FR, von Bossanyi P, Dietzmann K, Kunz WS. Impaired mitochondrial oxidative phosphorylation in skeletal muscle of the dystrophin-deficient mdx mouse. *Mol Cell Biochem.* 1998;183:87-96.

15. Percival JM, Siegel MP, Knowels G, Marcinek DJ. Defects in mitochondrial localization and ATP synthesis in the mdx mouse model of Duchenne muscular dystrophy are not alleviated by PDE5 inhibition. *Hum Mol Genet.* 2012;22:153-167.

16. Tarnopolsky MA, Mahoney DJ, Vajsar J, et al. Creatine monohydrate enhances strength and body composition in Duchenne muscular dystrophy. *Neurology.* 2004;62:1771-1777.

17. Srivastava NK, Pradhan S, Mittal B, Gowda GAN. High resolution NMR based analysis of serum lipids in Duchenne muscular dystrophy patients and its possible diagnostic significance. *NMR Biomed.* 2010;23:13-22.

18. Srivastava NK, Mukherjee S, Sinha N. Alteration of phospholipids in the blood of patients with Duchenne muscular dystrophy (DMD): in vitro, high resolution 31P NMR-based study. *Acta Neurol Belg.* 2016;116:573-581.

19. Gillet B, Doan BT, Verre-Serrie C, et al. In vivo 2D 1H NMR of mdx mouse muscle and myoblast cells during fusion: Evidence for a characteristic signal of long chain fatty acids. *Neuromuscul Disord.* 1993;3:433-438.

20. Touboul D, Piednoël H, Voisin V, et al. Changes of phospholipid composition within the dystrophic muscle by matrix-assisted laser desorption/ionization mass spectrometry and mass spectrometry imaging. *Eur J Mass Spectrom.* 2004;10:657-659.

21. Sharma U, Atri S, Sharma MC, Sarkar C, Jagannathan NR. Skeletal muscle metabolism in Duchenne muscular dystrophy (DMD): an in-vitro proton NMR spectroscopy study. *Magn Reson Imaging.* 2003;21:145-153.

22. Srivastava NK. Proton Nuclear Magnetic Resonance ((1)H NMR) Spectroscopy-Based Analysis of Lipid Components in Serum/Plasma of Patients with Duchenne Muscular Dystrophy (DMD). *Methods Mol Biol.* 1687;2018:195-204.

23. Srivastava NK, Yadav R, Mukherjee S, Pal L, Sinha N. Abnormal lipid metabolism in skeletal muscle tissue of patients with muscular dystrophy: In vitro, high-resolution NMR spectroscopy based observation in early phase of the disease. *Magn Reson Imaging.* 2017;38:163-173.

24. Sébrié C, Gillet B, Lefaucheur JP, Sebille A, Beloeil JC. Mouse muscle regeneration: an in vivo 2D 1H magnetic resonance spectroscopy (MRS) study. *FEBS Lett.* 1998;423:71-74.

25. Milad N, White Z, Tehrani AY, Sellers S, Rossi FMV, Bernatchez P. Increased plasma lipid levels exacerbate muscle pathology in the mdx mouse model of Duchenne muscular dystrophy. *Skeletal Muscle.* 2017;7:809.

26. Timpani CA, Hayes A, Rybalka E. Revisiting the dystrophin-ATP connection: How half a century of research still implicates mitochondrial dysfunction in Duchenne Muscular Dystrophy aetiology. *Med Hypotheses.* 2015;85:1021-1033.

27. McIntosh LM, Baker RE, Anderson JE. Magnetic resonance imaging of regenerating and dystrophic mouse muscle. *Biochem Cell Bio.* 1998;76:532-541.

28. Carnwath JW, Shotton DM. Muscular dystrophy in the mdx mouse: Histopathology of the soleus and extensor digitorum longus muscles. *J Neurol Sci.* 1987;80:39-54.

29. Martins-Bach AB, Bloise AC, Vainzof M, Rahnamaye Rabbani S, Rabbani SR. Metabolic profile of dystrophic mdx mouse muscles analyzed with in vitro magnetic resonance spectroscopy (MRS). *Magn Reson Imaging.* 2012;30:1167-1176.

30. Pastoret C, Sebille A. mdx mice show progressive weakness and muscle deterioration with age. *J Neurol Sci.* 1995;129:97-105.

31. Slotboom J, Bovée WMMJ. Adiabatic slice-selective rf pulses and a single-shot adiabatic localization pulse sequence. *Concepts Magn Reson.* 1995;7:193-217.

32. Ogg RJ, Kingsley PB, Taylor JS. WET, a T1- and B1-insensitive water-suppression method for in vivo localized 1H NMR spectroscopy. *J Magn Reson B.* 1994;104:1-10.

33. Ramaswamy V, Hooker JW, Withers RS, Nast RE, Brey WW, Edison AS. Development of a 13C-optimized 1.5-mm high temperature superconducting NMR probe. *J Magn Reson.* 2013;235:58-65.

34. Carr HY, Purcell EM. Effects of Diffusion on Free Precession in Nuclear Magnetic Resonance Experiments. *Phys Rev.* 1954;94:630-638.

35. Meiboom S, Gill D. Modified Spin-Echo Method for Measuring Nuclear Relaxation Times. *Rev Sci Instrum.* 1958;29:688-691.

36. Clendinen CS, Lee-McMullen B, Williams CM, et al. 13C NMR Metabolomics: Applications at Natural Abundance. *Anal Chem.* 2014;86:9242-9250.

37. Beckonert O, Coen M, Keun HC, et al. High-resolution magic-angle-spinning NMR spectroscopy for metabolic profiling of intact tissues. *Nat Protoc.* 2010;5:1019-1032.

38. Vohra RS, Mathur S, Bryant ND, Forbes SC, Vandenborne K, Walter GA. Age-related T 2changes in hindlimb muscles of mdxmice. *Muscle Nerve.* 2015;53:84-90.

39. Delaglio F, Grzesiek S, Vuister GW, Zhu G, Pfeifer J, Bax A. NMRPipe: a multidimensional spectral processing system based on UNIX pipes. *J Biomol NMR.* 1995;6:277-293.

40. Robinette SL, Ajredini R, Rasheed H, et al. Hierarchical Alignment and Full Resolution Pattern Recognition of 2D NMR Spectra: Application to Nematode Chemical Ecology. *Anal Chem.* 2011;83:1649-1657.

41. Wong JWH, Durante C, Cartwright HM. Application of Fast Fourier Transform Cross-Correlation for the Alignment of Large Chromatographic and Spectral Datasets. *Anal Chem.* 2005;77:5655-5661.

42. Dieterle F, Ross A, Schlotterbeck G, Senn H. Probabilistic Quotient Normalization as Robust Method to Account for Dilution of Complex Biological Mixtures. Application in 1H NMR Metabonomics. *Anal Chem.* 2006;78:4281-4290.

43. Mosconi E, Mosconi E, Fontanella M, et al. Investigation of adipose tissues in Zucker rats using in vivo and ex vivo magnetic resonance spectroscopy. *J Lipid Res.* 2011;52:330-336.

44. Wold S, Esbensen K, Geladi P. Principal component analysis. *Chemom Intell Lab Syst.* 1987;2:37-52.

45. Lindgren F, Geladi P, Wold S. The kernel algorithm for PLS. *J Chemometrics.* 1993;7:45-59.

46. Shapiro SS, Wilk MB. An analysis of variance test for normality (complete samples). *Biometrika.* 1965;52:591-611.

47. Walter G, Cordier L, Bloy D, Lee Sweeney H. Noninvasive monitoring of gene correction in dystrophic muscle. *Magn Reson Med.* 2005;54:1369-1376.

48. Xu S, Pratt SJP, Spangenburg EE, Lovering RM. Early metabolic changes measured by 1H MRS in healthy and dystrophic muscle after injury. *J Appl Physiol.* 2012;113:808-816.

49. Ulrich EL, Ulrich EL, Akutsu H, et al. BioMagResBank. *Nucleic Acids Res.* 2007;36:D402-D408.

50. Willcocks RJ, Rooney WD, Triplett WT, et al. Multicenter prospective longitudinal study of magnetic resonance biomarkers in a large duchenne muscular dystrophy cohort. *Ann Neurol.* 2016;79:535-547.

51. Forbes SC, Willcocks RJ, Triplett WT, et al. Magnetic Resonance Imaging and Spectroscopy Assessment of Lower Extremity Skeletal Muscles in Boys with Duchenne Muscular Dystrophy: A Multicenter Cross Sectional Study. Taneja R, ed. *PLoS One.* 2014;9:e106435.

52. Arpan I, Forbes SC, Lott DJ, et al. T2mapping provides multiple approaches for the characterization of muscle involvement in neuromuscular diseases: a cross-sectional study of lower leg muscles in 5–15-year-old boys with Duchenne muscular dystrophy. *NMR Biomed.* 2012;26:320-328.

53. Johnston JH, Kim HK, Merrow AC, et al. Quantitative Skeletal Muscle MRI: Part 1, Derived T2 Fat Map in Differentiation Between Boys With Duchenne Muscular Dystrophy and Healthy Boys. *Am J Roentgenol.* 2015;205:W207-W215.

54. Willcocks RJ, Arpan IA, Forbes SC, et al. Longitudinal measurements of MRI-T2 in boys with Duchenne muscular dystrophy: Effects of age and disease progression. *Neuromuscul Disord.* 2014;24:393-401.

55. Hollingsworth KG, Garrood P, Eagle M, Bushby K, Straub V. Magnetic resonance imaging in duchenne muscular dystrophy: Longitudinal assessment of natural history over 18 months. *Muscle Nerve.* 2013;48:586-588.

56. Gramolini AO, Gramolini AO, Jasmin BJ, Jasmin BJ. Duchenne muscular dystrophy and the neuromuscular junction: The utrophin link. *Bioessays.* 1997;19:747-750.

57. Villalta SA, Rinaldi C, Deng B, Liu G, Fedor B, Tidball JG. Interleukin-10 reduces the pathology of mdx muscular dystrophy by deactivating M1 macrophages and modulating macrophage phenotype. *Hum Mol Genet.* 2011;20:790-805.

58. Touboul D. Lipid imaging by gold cluster time-of-flight secondary ion mass spectrometry: application to Duchenne muscular dystrophy. *J Lipid Res.* 2005;46:1388-1395.

59. Lott DJ, Forbes SC, Mathur S, et al. Assessment of intramuscular lipid and metabolites of the lower leg using magnetic resonance spectroscopy in boys with Duchenne muscular dystrophy. *Neuromuscul Disord.* 2014;24:574-582.

60. Tuazon MA, Henderson GC. Fatty acid profile of skeletal muscle phospholipid is altered in mdx mice and is predictive of disease markers. *Metab Clin Exp.* 2012;61:801-811.

61. Piperi C, Papapanagiotou A, Kalofoutis C, et al. Altered long chain fatty acids composition in Duchenne muscular dystrophy erythrocytes. *In Vivo.* 2004;18:799-802.

62. Benabdellah F, Yu H, Brunelle A, Laprévote O, La Porte De S. MALDI reveals membrane lipid profile reversion in MDX mice. *Neurobiol Dis.* 2009;36:252-258.

63. Griffin JL, Williams HJ, Sang E, Clarke K, Rae C, Nicholson JK. Metabolic Profiling of Genetic Disorders: A Multitissue 1H Nuclear Magnetic Resonance Spectroscopic and Pattern Recognition Study into Dystrophic Tissue. *Anal Biochem.* 2001;293:16-21.

64. Morrison-Nozik A, Anand P, Zhu H, et al. Glucocorticoids enhance muscle endurance and ameliorate Duchenne muscular dystrophy through a defined metabolic program. *Proc Natl Acad Sci USA.* 2015;201512968–10. https://doi.org/10.1073/pnas.1512968112

65. McIntosh LM, Garrett KL, Megeney L, Rudnicki MA, Anderson JE. Regeneration and myogenic cell proliferation correlate with taurine levels indystrophin- and MyoD-deficient muscles. *Anat Rec.* 1998;252:311-324.

66. Rodríguez-Cruz M, Sanchez R, Escobar RE, et al. Evidence of insulin resistance and other metabolic alterations in boys with duchenne or becker muscular dystrophy. *Int J Endocrinol.* 2015;2015(4):1-8.

67. Raith M, Valencia RG, Fischer I, et al. Linking cytoarchiture to metabolism: sarcolemma-associated plectin affects glucose uptake by destabilizing microtubule networks in mdx myofibers. *Skeletal Muscle* 2013;3(1):14.

68. Stapleton DI, Lau X, Flores M, et al. Dysfunctional Muscle and Liver Glycogen Metabolism in mdx Dystrophic Mice. Gaetano C, ed. *PLoS ONE* 2014;9(3): e91514. https://doi.org/10.1371/journal.pone.0091514

SUPPORTING INFORMATION

Additional supporting information may be found online in the Supporting Information section at the end of the article.